



Carbon-Tunable p-type ZnO Nanoparticles for Enhanced Photocatalytic Removal of Eriochrome Black T

Auwal Yushau ^{a, b}, Umar Ibrahim Gaya ^{a, b}, *

^aDepartment of Pure and Industrial Chemistry, Faculty of Physical Sciences, Bayero University Kano, P.M.B 3011, 700241 Kano, Kano State, Nigeria

^bDirectorate of Science, National Agency for Science and Engineering Infrastructure, Idu Industrial Layout, P.M.B. 391, Garki, Abuja, Nigeria

* Corresponding author: E-mail: uigaya.chm@buk.edu.ng

ABSTRACT

Zinc oxide-mediated photocatalysis is a promising alternative to TiO₂ photocatalysis, especially for the purpose of removal of recalcitrant organic dye pollutants. Highly crystalline, nanoscopic carbon doped ZnO was successfully synthesized via combined precipitation and mechanochemical approach and characterized using x-ray diffraction (XRD), scanning electron microscopy (SEM), energy dispersive x-ray (EDX) and Fourier transform infrared (FTIR) spectrometry. The obtained photocatalysts depict plate-like morphology and hexagonal wurtzite structure. The XRD, SEM, and FTIR analyses were in good agreement with EDX results. The 5wt % C-doped ZnO showed remarkable visible light-photocatalytic activity based on the degradation of Eriochrome Black T (EBT) and exhibits the best point of zero charge (pHpzc) for a favorable adsorption equilibrium. This degradation process was optimized at 97 % using response surface methodology (RSM) using a 0.1 g C-ZnO, 5.00 mg/L EBT and pH 11. The associated kinetic data fit the pseudo-first-order kinetic model. The resulting C-ZnO was a p-type with a good pH at zero-point charge that permits the substantial removal of EBT by C-doped under visible light irradiation over a wide range of initial pH.

ARTICLE INFO

Keywords:

p-type ZnO
Doping,
Mechanochemical,
Photocatalysis,
RSM
Eriochrome Black T

Received: 2023-02-22

Accepted: 2023-02-28

ISSN: 2651-3080

DOI: 10.54565/jphcfum.1253804

Introduction

Over the decades, semiconductor photocatalysis has been recognized as a game-changing environmental remediation technology due to its unrivalled removal capacity and mineralization efficiency for a broad spectrum of non-biodegradable organic compounds [1-6]. Interest in zinc oxide semiconductor has heightened due to its availability, non-toxicity and inexpensiveness [7, 8] despite its wide band gap (3.37 eV), susceptibility to photocorrosion and rapid recombination [9]. Non-metal doping can reduce the recombination rate and enhance the efficiency of this semiconductor photocatalyst via a redshift of band gap edges [10, 11].

Unless abated, azo dyes such as Eriochrome Black T (EBT) will pose a costly or laborious remediation process [6] and considerable health risk to human and aquatic life [12, 13] due to their complex molecular structure, chemical stability, non-biodegradable and high solubility in water [14]. Because they are commonly used in textiles, biological staining, research and teaching laboratories, coupled with the risk of uncontrolled release, these dyes

have increasingly become environmentally important [15,16].

Previous works under ultraviolet irradiation, reported a poor efficiency of EBT removal over ZnO, with performance figures ranging from 62 % [17] to 83 % [2, 18,] at alkaline conditions. The enhancement of the activity of ZnO photocatalyst is imperative to shift the light absorption into the visible light region of the electromagnetic radiation. Non-metal-doping using S, N or C can both extend visible light absorption significantly and suppress the recombination of photogenerated charge carriers. Carbon is known to be an efficient dopant for visible light ZnO photocatalysis and the enhancement of the performance of photoelectrochemical fuel cell due to its lower energy for substitution and comparable size relative to oxygen [19, 20, 21]. In fact, the nanosized C-doped ZnO has consistently shown outstanding enhancement in photocatalytic degradation, even up to three times than pure ZnO [22, 23, 24]. This is evident in the photocatalytic degradation of tetracycline over C-doped

ZnO nanoparticle which significantly outperformed that of the bare ZnO [20].

Basically, the photoefficiency of ZnO is greatly influenced by the pH at point of zero charge (pH_{pzc}). This pH is crucial for the prediction of the charge on the photocatalyst surface during photocatalytic removal [25]. It governs the surface characteristics and size of the aggregated catalyst as it interacts with the charge of organic molecules, governs its adsorption capacity and the population of hydroxyl radical for the photocatalytic degradation of organic pollutants [26, 27]. Firstly, despite the existence of related works, the photocatalytic removal of EBT over C-doped ZnO nanoparticle has not been reported. Secondly, to the best of our knowledge, the influence of C content of ZnO on its point of zero charge and consequently the photocatalytic efficiency for EBT degradation has not been studied. We mechanochemically synthesized C-doped p-type ZnO photocatalyst for the degradation of Eriochrome Black T and optimized the factors affecting the process using a face-centered central composite design (FCCD).

Experimental Method

2.1. Chemicals

Zinc acetate dihydrate ($Zn(CH_3COO)_2 \cdot 2H_2O$, 98%), sulfuric acid (H_2SO_4 , 99%) and Eriochrome Black T ($C_{20}H_{12}N_3O_9S$, 99%) were supplied by Sigma Aldrich, Canada, while urea ($(NH_2)_2CO$, 99%), sodium hydroxide (NaOH, 98%) and ammonium hydroxide (NH_4OH , 98%) were obtained from BDH, Poole, England. All chemicals were used as received from the manufacturers without further purification. Stock solutions of EBT were prepared using deionized distilled water and used fresh. All experiments were carried out in a 30 cm long, 1 L capacity, round bottom batch photoreactor, maintained at 298 K. The visible light source was a 300 W Xenon lamp emitting at 400 nm. This lamp was jacketed in cylindrical quartz glass, dipping down the reactor bottom. The structural formula of EBT is shown in Fig. 1.

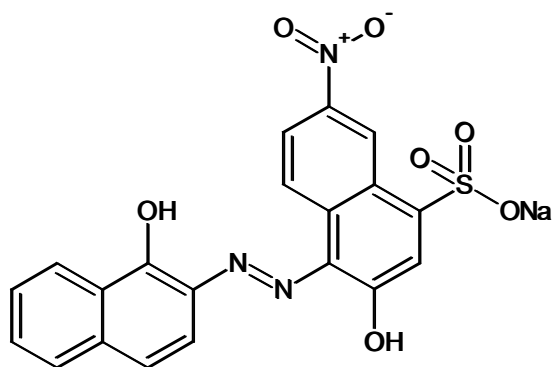


Fig. 1 Molecular structures of EBT

2.2. Synthesis of C-doped ZnO

The undoped ZnO was prepared using a precipitation method. Zinc acetate dihydrate ($Zn(CH_3COO)_2 \cdot 2H_2O$) (66.69 g) was dissolved in 500 ml of deionized water by vigorously stirring till a homogeneous solution was obtained. Then exactly 12.15 g of sodium hydroxide (NaOH) were added at a constant rate to the preceding solution with vigorous stirring at 80 °C and pH 8. The resulting precipitate was aged for 24 h, recovered by centrifugation, washed several times with deionized water

and filtered under vacuum to obtain a ZnO precursor. This precursor was dried overnight in an oven at 140 °C, calcined in a muffle furnace at 450 °C for 4 h, and cooled to room temperature to obtain a bare ZnO.

The C-doped ZnO was obtained by mechanochemical grinding of ZnO (10 g) and urea (1-20 wt % versus ZnO) in an agate mortar for 5 h [20]. The mixture was calcined in a muffle furnace at 450 °C for 4 h to remove nitrogen. The resulting material was ground to a fine powder and then labeled as a C-doped ZnO photocatalyst.

2.3. Photocatalyst Characterization

The particle size, crystal phase, lattice strain and purity of the synthesized photocatalysts were analyzed using diffractograms from Philips X pert Pro diffractometer operated with a CuK_{α} radiation ($\lambda = 1.54468 \text{ \AA}$) in the 2 θ range 5-70 ° at 30 kV, 30 mA and scanning rate of 2 min. Rietveld refinement of the structure was performed using the WINPLOTR package of FullProf suite version 2018. The lattice parameters such as spacing distance between the adjacent planes in the miller indices d_{hkl} , lattice constant a, b and c, and volume of the unit cell for the undoped ZnO and C-doped ZnO photocatalysts were calculated using eq. (1-4). The calculated values for the synthesized catalysts were compared to the unit cell parameters for the standard undoped ZnO (JCPDS 070-8072) and C-doped ZnO (JCPDS 071-6424) [28].

$$a = b = \frac{\lambda}{\sqrt{2} \sin \theta \sin \theta} \quad (1)$$

$$c = \frac{\lambda}{\sin \theta \cos \theta} \quad (2)$$

$$d_{hkl} = \frac{abc}{\sqrt{a^2c^2(h^2 + hk + k^2) + 3\left(\frac{ab}{c}\right)^2}} \quad (3)$$

$$v = 0.866 \times a^2 \times c \quad (4)$$

Where a, b, and c are the lattice constants, λ is the wavelength of x-ray radiation (1.5406 Å), θ is Bragg's angle, d_{hkl} is the d-spacing hkl is the miller indices, and V is the volume of a unit cell.

The average crystalline size has been estimated using Debye-Scherrer (eq. 5). The surface area and the number of unit cell per particle for the undoped ZnO and the C-doped ZnO were calculated from the eq. (6-8), respectively.

$$D = \frac{k\lambda}{\beta \cos \epsilon} \quad (5)$$

$$N = \frac{4}{3\pi \times \frac{4}{\gamma v}} \quad (6)$$

$$SSA = \frac{600c}{D \times \rho} \quad (7)$$

$$N = \frac{4}{3\pi \times \frac{4}{\gamma v}} \quad (8)$$

Where D is the average particle size, k is the Debye-Scherrer constant (0.89), λ is the wavelength of the x-ray radiation, β is the full width at half maximum intensity

(FWHM), θ is the diffraction angle at the position of peak maximum, SSA is the specific surface area, SA is the surface area, ρ is the density of ZnO (5.69 gcm^{-3}) and C-doped ZnO (5.68 gcm^{-3}) and N is the number of unit per particles.

The surface morphology of the synthesized photocatalysts was recorded on LEICA Stereo scan-440 interfaced with Phoenix proxy energy dispersive x-ray spectrometer. The facility was operated at the same scale ($30 \mu\text{m}$), magnification (2,500) and accelerating voltage (15 kV). The FTIR spectra of the catalysts were recorded using Agilent Cary 630 diamond total attenuated reflectance Fourier transform infrared spectrometer (ATR-FTIR).

The elemental composition for the undoped and C-doped ZnO photocatalysts was recorded using an E-max-60 spectrometer interfaced with SEM. The band gap values of the catalysts were calculated using the Schuster-Kubelka-Munk relation from the electronic data recorded over a wavelength range of 200-800 nm on a Lambda 35 Perkin Elmer UV-Visible spectrophotometer.

2.4. Surface Area of the Photocatalysts

The surface area (S.A) of the synthesized photocatalysts was determined from the x-ray diffraction (XRD) row data. The S.A for the bare and C-doped ZnO photocatalyst has been estimated using equation 7 and 8 respectively [29].

$$\overline{\text{SSA}} = \frac{\text{SA}}{V \times \rho} \quad (7)$$

$$\overline{\text{SSA}} = \frac{6000}{D \times \rho} \quad (8)$$

Where SSA is the specific surface area, SA is the surface area, ρ is the density of ZnO (5.69 gcm^{-3}) and C-doped ZnO (5.68 gcm^{-3}).

2.5. Band Gap Measurement

The band gap energy (E_g) values for the undoped and C-doped ZnO photocatalysts were obtained from the electronic data recorded over the wavelength range 200-800 nm on the Lambda 35 Perkin Elmer UV-Visible spectrophotometer. However, E_g values for the synthesized catalysts were calculated using the Schuster-Kubelka-Munk relation (eq. 9) [29].

$$\overline{(\alpha h\nu)^{\frac{1}{n}}} = K \overline{(h\nu - E_g)} \quad (9)$$

Where $\overline{\alpha}$ is the absorption coefficient obtained from Beer's law, h is the Planck's constant, $\overline{\nu}$ is the frequency of vibration, K is a proportionality constant and $\overline{E_g}$ is the band gap energy of the semiconductor photocatalyst. The $\overline{E_g}$ values were calculated from the intercept of the plot of $\overline{(\alpha h\nu)^{\frac{1}{n}}}$ against $\overline{h\nu}$. If scattering is insignificant the term $\overline{\alpha h\nu}$ is proportional to a function of reflectance $\overline{[F(R)(\alpha h\nu)]}$. Since the semiconductor ZnO used in this experiment is a direct band gap allowed sample transition and thus the denominator of the exponent $n = \frac{1}{2}$.

2.6. Determination pH_{pzc} of the Photocatalysts

The point of zero charge (pH_{pzc}) is the point at which the net charge on the photocatalyst surface is zero or neutral. It was determined using the widely used drift method [29, 30], for both the undoped ZnO and C-doped ZnO catalysts. In this method, 0.1 molL^{-1} KCl was prepared and its initial was adjusted between 2.0 to 12 by the addition of either NaOH or HCl. To a 25 ml of the KCl solution, 50 mg of sample was added, shaken mechanically for 3 h, filtered and then the final pH (pH_{final}) of the solution was recorded and plotted against the initial pH ($\text{pH}_{\text{initial}}$). The point at which the curve of the plot intersects the x-axis was taken as the pH_{pzc} of the sample.

2.7. Photocatalytic Experiments

All experiments were conducted in an immersion well photoreactor [31] made of a 7 cm diameter, 30 cm long cylindrical quartz glass housed in a 1 L round bottom flask having an effective volume of 0.6 L. The visible light source is a 300 W Xenon lamp emitting light of 120 mW/cm^2 intensity at 400 nm. Samples were collected through a sample port.

Exactly 400 ml aqueous solution of the desired amount of EBT and C-doped ZnO photocatalyst were added to the photoreactor, and the pH of the suspension was adjusted using 0.5 molL^{-1} NaOH and H_2SO_4 . This mixture was exposed to irradiation under continuous stirring at room temperature ($25 \text{ }^\circ\text{C}$) for 160 min. After every 20 min, an aliquot was filtered using $0.45 \mu\text{m}$ cellulose nitrate filter and analyzed for residual concentration of EBT at 564.38 nm using a Lambda 35 Perkin Elmer UV-Vis spectrophotometer. The percent photodegradation efficiency (% D) was calculated using eq. (10).

$$\overline{D\%} = \frac{[\text{EBT}]_0 - [\text{EBT}]_t}{[\text{EBT}]_0} \times 100 \quad (10)$$

Where $[\text{EBT}]_0$ and $[\text{EBT}]_t$ are the initial and final concentration of Eriochrome Black T, and t is the irradiation time. Possible background reactions such as dark adsorption and photolysis over the undoped and doped ZnO catalysts were also examined. These were compared with photocatalysis over the C-doped ZnO photocatalyst.

To find the optimum conditions of the EBT photocatalytic degradation, a response surface methodology (RSM) based on a three-level-three-variable face-centered central composite design (FCCD). These independent variables are the initial EBT concentration (A), catalyst loading (B) and initial pH (C) operated at three levels (low, central, high) coded -1, 0 and +1 (Table 1). Other variables such as agitation speed, light intensity, oxygen pressure and delivery volume were maintained constant. A total of 20 experiments (N) were performed based on the formula $N = 2^n + 2n + 6$. Where n is the number of variables. The % D obtained from these experiments were processed using Design Expert software version 6.0.6 to obtain the predicted responses, response surface and regression model for the EBT degradation.

To determine the kinetic scheme of the EBT degradation over C-doped ZnO photocatalyst, experiments were run at

the optimal operating conditions obtained from the response surface methodology. Similar experiments were performed at different initial concentrations (20.00, 15.00, 10.00, and 5.00 mgL⁻¹) respectively, and the data were fitted into the integrated rate equations.

RESULTS AND DISCUSSIONS

Table 2 shows the Kruskal-Wallis test results that were carried out to check whether there was a difference between the CLIK, DMIR, ERGA, HELI, NURD, KZIL, OSMA, PALU, PTRG and SURG stations over time. Results indicated that significant differences were observed in most of the stations (p value <0.05) by year. In the table, * is used for years with no difference.

Table 1 Initial experimental levels and codes of variables

Variable	Notation	Levels (Codes)		
Initial EBT concentration (mgL ⁻¹)	A	5 (-1)	10 (0)	20 (+1)
Catalyst loading (gL ⁻¹)	B	0.04 (-1)	0.06 (0)	0.1 (+1)
Initial pH	C	3 (-1)	8 (0)	11 (+1)

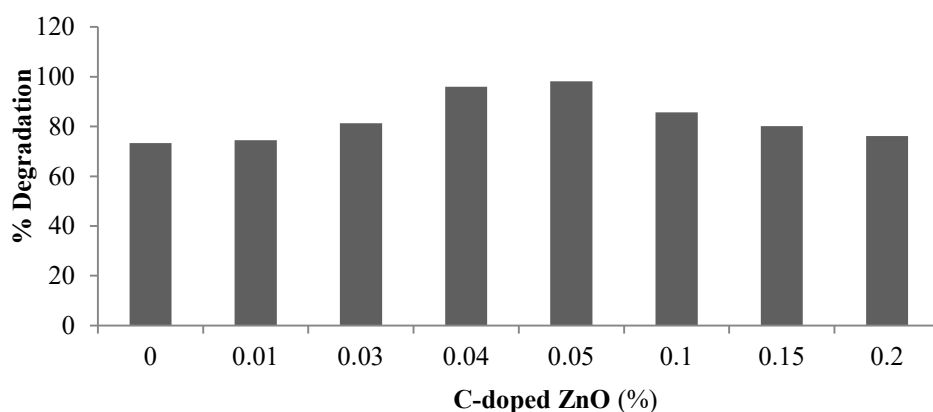


Fig. 2 Variation of EBT removal with the C content of ZnO

Table 2 The geometrical lattice parameters and crystal structure of undoped and C-doped ZnO from Rietveld refinement calculation

Photocatalyst	d ₁₀₀ (Å)	Lattice parameters in (Å)		c/a ratios	Crystal structure	Volume of a unit cell (Å ³)	Unit cells per particle
		a = b	c				
Bare ZnO	2.8115	3.2466	5.2031	1.6026	Hexagonal wurtzite	47.4939	1.2868
C-doped ZnO	2.8139	3.2495	5.2040	1.6015	Hexagonal wurtzite	47.5869	1.9721

3.1. Tuning ZnO Activity with Carbon

The performance of different amounts of carbon dopant in the degradation of Eriochrome Black T was evaluated using 10.00 mgL⁻¹ solution of EBT, 0.1gL⁻¹ ZnO catalysts with C content in the range of 0 to 20 %, and the results are displayed in Fig. 2. It can be seen that the photocatalytic degradation efficiency of EBT as the carbon content is increased from 0 to 5 %. A decline in the degradation efficiency was observed all through above 5 % carbon. Thus, 5 % C-doped ZnO was found to be the optimal amount of dopant when compared to the rest of the C-doped ZnO photocatalysts, and this amount was used in the other studies. The enhanced photocatalytic activity of the 5 wt% C-doped ZnO may be attributed to the creation of just enough shallow trapping sites for the charge carriers by the presence of C, which causes a difference in the surface arrival time of electron and hole pairs and prevents recombination [32].

3.2 Physicochemical Properties of the Photocatalysts

3.2.1. Particle Size, Surface Area and Crystallinity

The microstructure, crystal phase, purity, crystallite size and lattice strain for the synthesized photocatalysts, were determined using powder XRD. The obtained diffraction patterns are presented in Fig. 3 (a) and (b). From Fig. 3 (a), the Bragg's peaks at 2θ values of 31.8°, 34.4°, 36.3°, 47.6°, 56.7°, 62.9°, 66.5°, 68.0° and 69.1° correspond to the structural miller indices (100),(002), (101), (102), (110), (103), (200), (112), and (201) of undoped ZnO crystal plane. Similarly, the diffraction peaks observed at 2θ = 31.7°, 34.4°, 36.2°, 47.6°, 56.6°, 62.8°, 66.4°, 67.9° and 69.0° correspond to the (100), (002), (101), (102), (110), (103), (200), (112), and (201) reflection planes of the C-doped ZnO (Fig. 3b). The absence of impurity peaks is a clear indication of a single phase, low content of incorporated dopant and high purity of the synthesized photocatalysts.

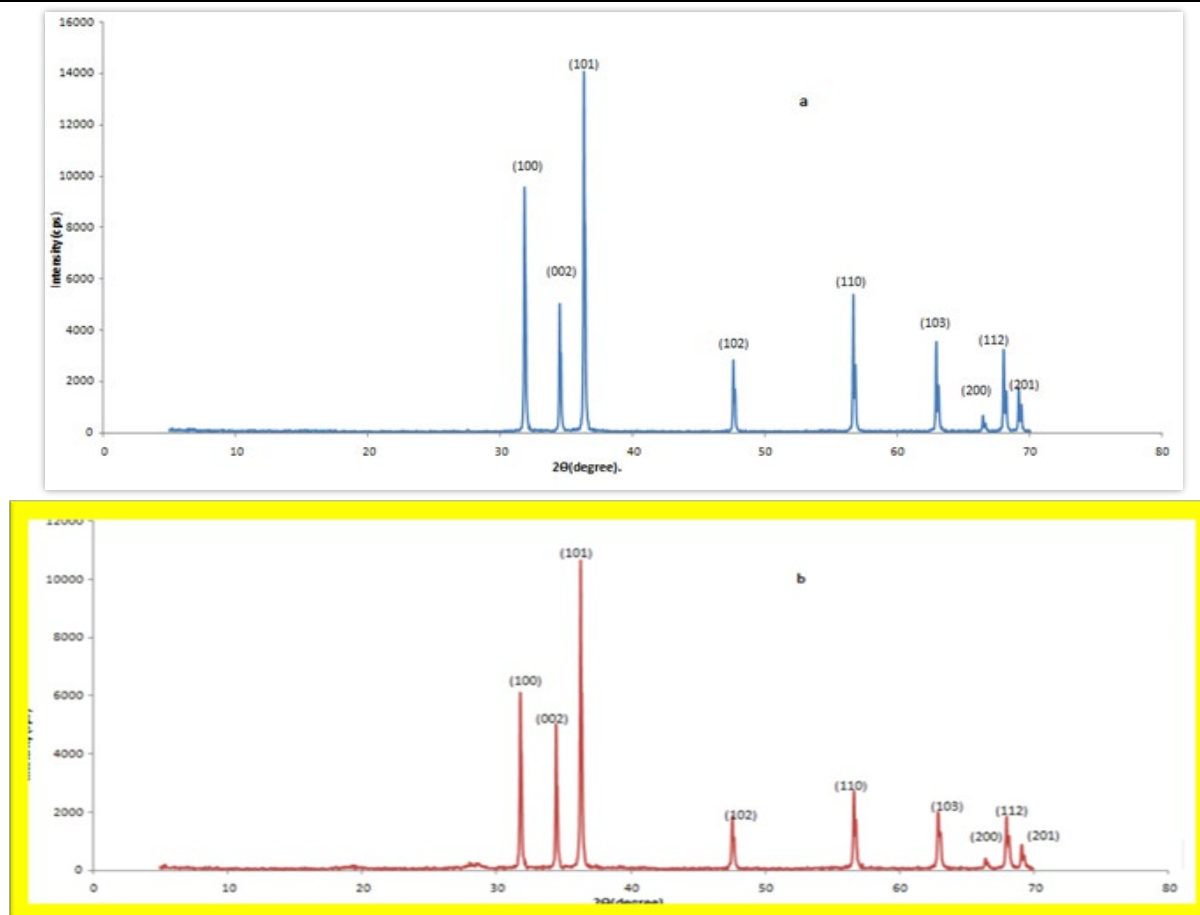


Fig. 3 The XRD diffraction patterns of photocatalysts. (a) Undoped ZnO (b) C-doped ZnO

The obtained XRD patterns for the bare ZnO and the C-doped ZnO matched the standard hexagonal wurtzite structure of ZnO (JCPDS 01-070-8072). The unit cell parameters calculated based on ZnO lattice planes (100) and (002) (Table 2) agree with the standard lattice parameters ($a=3.2465\text{\AA}$ and $c=5.2030\text{\AA}$; JCPDS Card no; 070-8072) and ($a=3.2494\text{\AA}$ and $c=5.2038\text{\AA}$; JCPDS Card no; 01-071-6424), respectively. The values calculated (Table 2) showed slight increases in the unit cell parameters including the spacing distance and unit cell volume. This is because the ionic radius of C anion (69-76 pm) is greater than that of oxygen (57-66 pm) and the

substitution of $O_{(-11)}$ by $C_{(-1v)}$ will result in an unbalanced system charge that can only be made neutral via oxygen loss [32].

The high crystallinity of the as-prepared ZnO powders is indicated by the outstanding sharpness of diffraction peaks. Upon doping, the specific surface area of the C-doped ZnO observed (Table 3) increased from 34.6 to 51.6 (m^2g^{-1}) while the XRD-based particle size dropped from 30 to 20 nm. Interestingly, an increase in the surface area of C-doped ZnO photocatalysts has usually been linked to enhanced interfacial reactions [32].

Table 3 The size, surface area and band gap of the ZnO particles

Photocatalyst	D(nm)	Specific surface area (m^2g^{-1})	pH _{pzc}	Band gap (eV)
Bare ZnO	30.29	34.62	9.1	3.25
C-doped ZnO	20.48	51.58	7.4	3.01

3.2.2. Surface Morphology and Elemental Analysis

The surface morphology of the as-prepared undoped ZnO and C-doped ZnO is shown in Fig. 4. From the figure, aggregation of particles is seen in the undoped ZnO (Fig. 4

a) and agglomeration of the particles was pronounced for the doped ZnO (Fig. 4 b). This might be due to the addition of dopant and grinding operation during the synthesis [33].

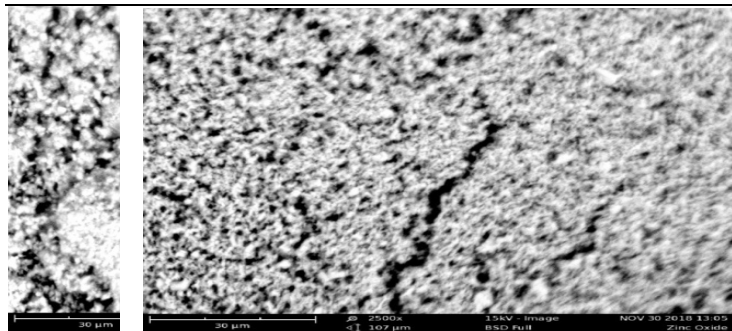


Fig. 4. The SEM Micrographs of undoped ZnO (left), and C-doped ZnO photocatalyst (right)

The presence of C atom with Zn and O atoms in the nanoparticles is substantiated by EDX analysis. The EDX spectra of bare and 5 % C-doped ZnO (which is the optimal catalyst) are presented in Fig 5. Prominent peaks were vividly observed at 0.57, 1.02, 8.65 and 9.65 keV. The X-ray energies of 0.57 and 1.02 keV respectively

represent the emission from the K-shell of oxygen and L-shell of Zn. The X-ray energies observed at 8.65 and 9.64 keV are additional emissions from the Zn core level. Carbon is indicated by the C 1s core level emission around 0.33 keV

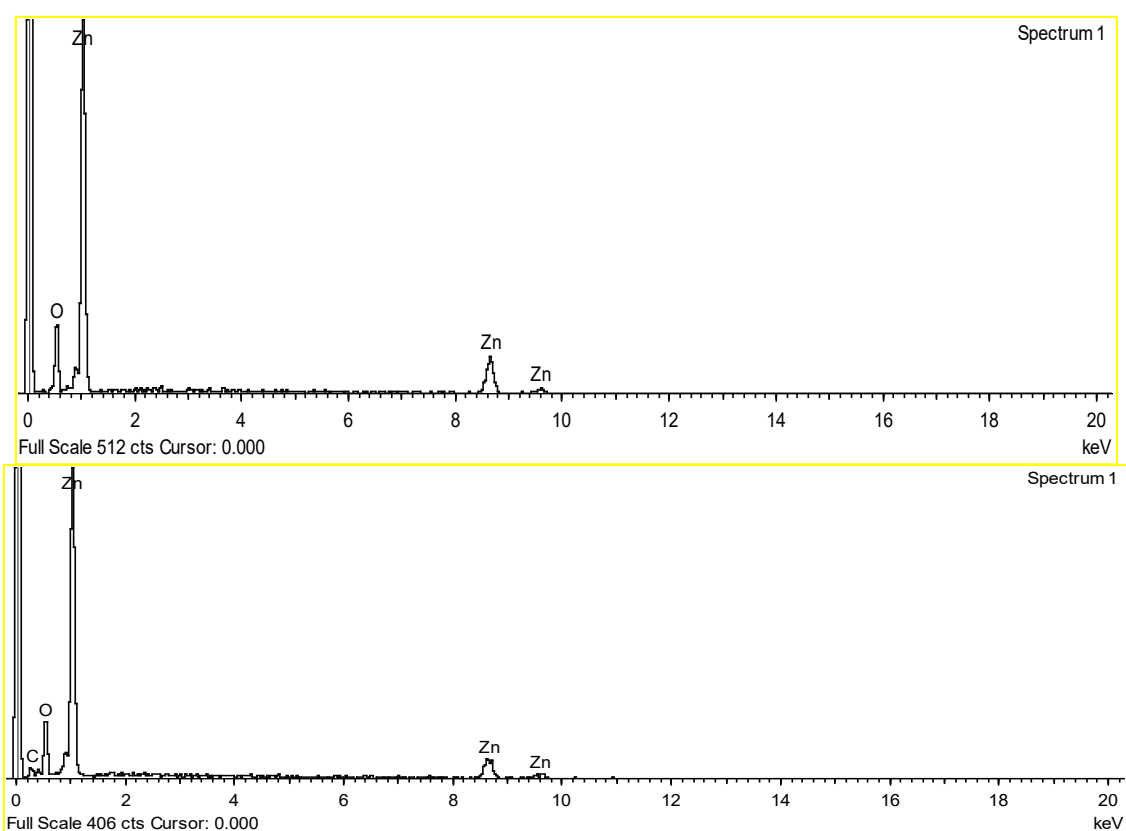


Fig. 5 The EDX spectra of undoped ZnO (top inset), and C-doped ZnO (bottom inset)

The weight and atomic percent composition of Zn and O atoms for undoped and Zn, O and C atoms in the C-doped ZnO are displayed in Table 4. Even though usually ZnO is considered as an n-type semiconductor where most defects

are interstitial zinc and oxygen vacancy, our results showed the deficiency of zinc and excess of oxygen which implies the existence of interstitial oxygen and the less observed p-type semiconducting ZnO nanoparticles.

Table 4 Weight and Atomic percentage of the constituents of undoped and C-doped ZnO photocatalyst

Element	Undoped ZnO		C-doped ZnO	
	Wt%	At%	Wt%	At%
CK	-	-	5.94	3.50
OK	19.99	51.51	22.02	53.88
ZnL	80.01	49.49	72.04	42.62
Total	100 %		100 %	

3.2.3. Fourier Transform Infrared Spectroscopy

The FTIR spectra of the undoped ZnO and 5 % C-doped ZnO nanoparticles are shown in Fig. 6 (a) and (b). The characteristic Zn-O bond stretching vibration is observed within the range of 629-699 cm^{-1} . The presence of C-O

stretching vibration is corroborated by the absorption band at 1521 cm^{-1} . This band is absent in the spectra of the undoped ZnO (Fig. 6 (a)). The FT-IR spectra did not present any of the characteristic N-H band at 3210 cm^{-1} which suggests that urea species were significantly eliminated by the thermal treatment during synthesis.

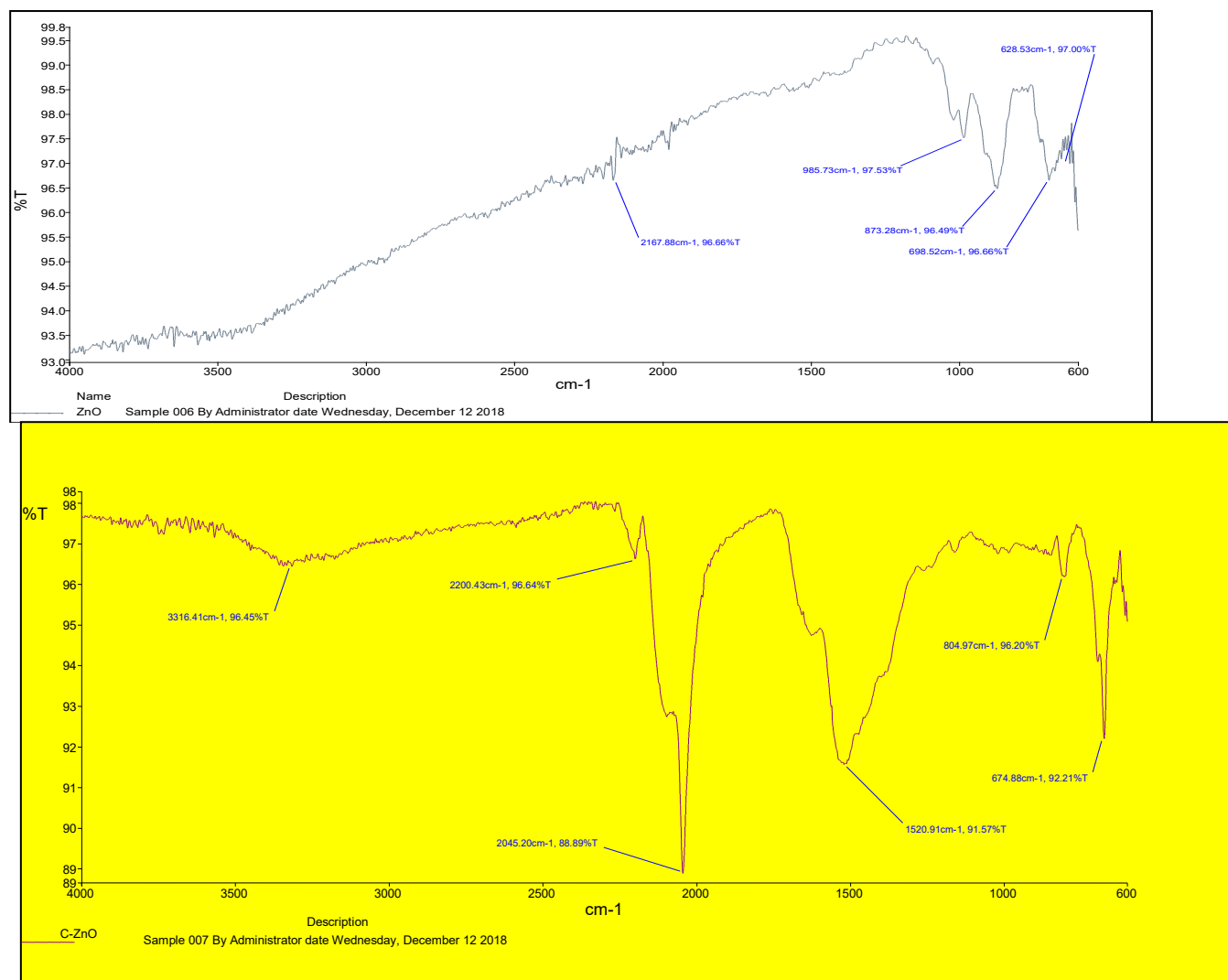


Fig. 6 The FTIR spectra of undoped ZnO (top), C-doped ZnO (bottom)

3.2.4. Band Gap Determination

The band gap energies of the obtained ZnO photocatalysts were calculated from the absorption data using Kubelka-Munk's intercept of the plot of $(\alpha h\nu)^2$ against $h\nu$, as displayed in Fig. 7. The figure shows linearity in the vicinity of the band gap region for both the C-doped ZnO and that of the bare ZnO, revealing that the C-doping did not change the direct electron transition characteristics of the ZnO [32]. The band gap energy values for the undoped and C-doped ZnO photocatalysts were 3.25 and 3.01 eV,

respectively, confirming the ability of the former to relatively absorb more visible light. This shows that the C doping reduces the band gap energy of the bare ZnO nanoparticles due to the narrowing particle size, ease of charge-transfer process and increased adsorption capacity between the C-doped ZnO and pollutant [33]. The relatively easier the charge-transitions of the C-doped ZnO would indicate higher conductivity and potential for photoelectrochemical reactions in comparison to the undoped ZnO nanoparticles [34].

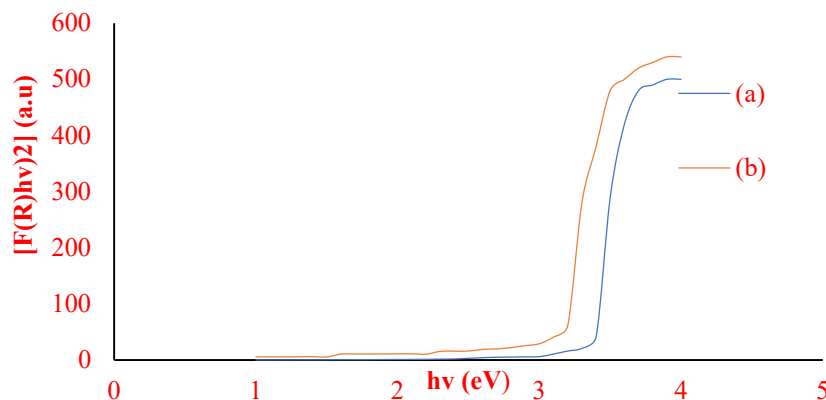
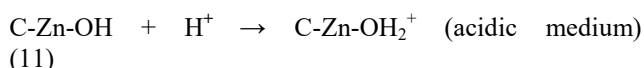


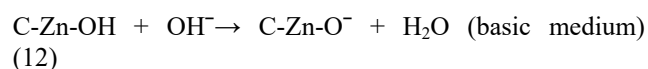
Fig. 7 Band gap plots for the ZnO powders. (a) Undoped ZnO. (b) Carbon-doped ZnO

3.3. Effect of the pH at Point of Zero Charge

Solution pH is an important parameter that affects the visible light photoactivity of ZnO photocatalysts during the organic compound removal [35]. The effect of pH at point of zero charge can be significant because the charge of ZnO surface and EBT can be changed with the shift in pH. The ZnO surface will prefer to dissolve in water to form a hydroxide layer (C-ZnO-OH). The surface formed can become charged by reacting with proton in acidic medium or hydroxyl ion in basic medium due to surface amphoteric reaction. Such process can be increased by the porous nature of the photocatalyst. As can be seen from the point of intersection of the abscissa of Fig. 8, the point of zero charge for the undoped ZnO is 9.1 while the estimated pH_{pzc} for the 5 % C-doped ZnO photocatalyst is 7.4. This means at any pH lower than 7.4 the hydroxylated ZnO surface would accept a proton to produce a positively charged surface according to eq. (11).



However, at high pH (> 7.4) the hydroxylated surface proton form a negatively charged surface according to eq. (12).



Therefore, the surface functional group of C-doped ZnO photocatalyst can be $C-ZnOH_2^+$, $C-ZnOH$ and $C-ZnO^-$ at $pH < pH_{pzc}$, pH_{pzc} , and $pH > pH_{pzc}$ respectively. On the other hand, the EBT is a basic base ($pK_a = 6$ and 11). In an acidic medium, more EBT molecules would tend to be positively charged while the lone pair electron of the phenolic and nitro group will be more available for hydrogen bonding (undissociated EBT) [36]. Consequently, at high pH ($pH \geq pK_a$), the EBT would be negatively charged. The enhanced photocatalytic degradation observed in this case might be attributed to the increase in the chemisorption adsorption and of course the enhanced generation of hydroxyl radicals.

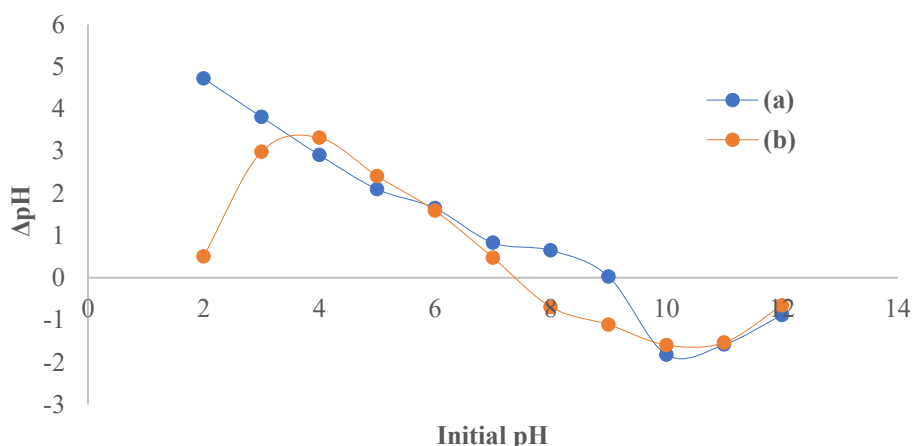


Fig. 8 A plot of ΔpH against $pH_{initial}$ for (a) undoped ZnO and (b) C-doped ZnO

3.4. Multivariate optimization

Experiments were conducted within different domains of initial EBT concentration (A), the mass of catalyst (B) and initial pH (C), and experimental and predicted responses are shown in Table 5. The predicted responses ($\%Y_{cal}$) based on coded levels fit the generic, second-order

polynomial model in eq. (12). The experimental optimum degradation efficiency (97 %) was achieved at $A = 5.00 \text{ mgL}^{-1}$, $B = 0.10 \text{ gL}^{-1}$ and $C = 11$.

$$\%Y_{cal} = +20.65 - 8.10A + 2.63B + 2.61C + 2.06A^2 - 0.13AB + 0.059AC - 0.30BC \quad (12)$$

Table 5 Experimental matrix and the corresponding degradation efficiencies

Run	Variables and code			Degradation efficiency (%)	
	A	B	C	(experimental)	(predicted)
1	5(-1)	0.04(-1)	3(-1)	88.09	86.09
2	20(+1)	0.04(-1)	3(-1)	70.45	70.34
3	5(-1)	0.1(+1)	3(-1)	91.88	92.51
4	20(+1)	0.1(+1)	3(-1)	75.66	75.92
5	5(-1)	0.04(-1)	11(+1)	92.18	92.10
6	20(+1)	0.04(-1)	11(+1)	77.18	76.28
7	5(-1)	0.1(+1)	11(+1)	97.18	97.02
8	20(+1)	0.1(+1)	11(+1)	79.24	80.67
9	5(-1)	0.06(0)	8(0)	90.65	92.41
10	20(+1)	0.06(0)	8(0)	76.88	76.20
11	10(0)	0.06(0)	8(0)	74.57	77.80
12	10(0)	0.1(+1)	8(0)	85.21	83.05
13	10(0)	0.06(0)	3(-1)	80.21	81.05
14	10(0)	0.06(0)	11(+1)	86.11	86.28
15	10(0)	0.06(0)	8(0)	79.09	82.25
16	10(0)	0.06(0)	8(0)	81.33	82.25
17	10(0)	0.06(0)	8(0)	87.27	82.25
18	10(0)	0.06(0)	8(0)	80.99	82.25
19	10(0)	0.06(0)	8(0)	85.68	82.25
20	10(0)	0.06(0)	8(0)	81,27	82.25

The positive sign in front of the terms in eq. (12) indicates synergistic effect which implies enhancement in the percent removal of EBT as opposed to the negative sign which indicates antagonistic effect [37]. Analysis of variance (ANOVA) was performed to check the model adequacy, by evaluating the sum of squares, degree of freedom, mean square, F-value and p-value and the results are shown in Table 6. From the Table, the model-value of 11.96 implies model significance and that there is only a 0.03 % chance of a noisy model F-value. The quality of the developed model is high given that $R^2 = 0.9815$. This implies that 97.18 % of the variations for the degradation of EBT dye were explained by the independent variables within the studied range. The lack of fit value of 0.54 is not significant relative to the pure error when p-value is 0.7424 (more than 0.05) which shows good predictability of the model. Meanwhile, the significance of the model

terms is proven by the small p-value (less than 0.0001). Therefore, the significant terms among the tested process parameters were solution pH > EBT concentration > second-order of solution pH > second-order of C-ZnO photocatalyst dosage > C-ZnO photocatalysts dosage > second-order of EBT concentration. Other model terms are insignificant as their p-value were greater than 0.1000 [38].

The coefficient of variance (C.V. = 3.33) is low, indicating a high precision and good reliability of the experimental values [39]. An adequate precision measure of 13.653, which is well above the value of 4, indicates an adequate signal. The regression model demonstrates a good relationship between independent variables, as both R^2 (0.985) are close to 1 [39]. In the study, the p-values of the major parameters (A and C) influencing the percentage removal of EBT are significant ($P < 0.05$). Similarly, the

interaction terms (AC), as well as the quadratic term (A^2), have probabilities less than 0.05, which indicates that they

significantly contribute to the degradation of EBT.

Table 6 The ANOVA for response surface reduced quadratic model

Source	Sum Square	of DF	Mean Square	F-value	P-value	Remarks
Model	821.78	7	91.31	11.96	0.0003	Significance
A	656.42	1	656.42	85.96	<0.0001	
B	68.91	1	68.91	9.02	0.0133	
C	69.23	1	69.23	9.12	0.0130	
A²	20.65	1	20.65	2.34	0.0331	
AB	0.15	1	0.15	0.018	0.7938	
AC	0.81	1	0.81	0.083	0.6730	
BC	22.75		22.75	3.45	0.0421	
Residual	76.37	12	7.64	-	-	
Lack of fit	26.73	7	5.36	0.54	0.7660	not significant
Pure error	49.5	5	9.92	-	-	
Corrected total	898.15	19	-	-	-	
Standard deviation	2.76	-	R ²	0.985	-	
Mean	83.08	-	Adj R ²	0.8384	-	
Coefficient of variance	3.33	-	Pred R ²	0.6750	-	
Press	291.94	-	Adeq. precision	13.653	-	

To validate the quadratic model obtained in this study, runs were individually performed and compared to the predicted results (Table 7). The experimental results were very close to the predicted values (94 %) confirming the reliability of the FCCD.

Table 7. Validation data of the quadratic model.

Run	Initial EBT concentration (mg/L)	Catalyst loading (g/L ⁻¹)	Initial pH	Experimental efficiency (%)	Predicted efficiency (%)
1	5.00	0.10	11.00	97.96 ± 0.11	97.02
2	10.00	0.06	8.00	78.99 ± 0.21	77.80
3	20.00	0.04	3.00	70.69 ± 0.45	70.34

Figure 9 (a) shows the three-dimensional response surface representing the influence of C-doped ZnO loading and initial EBT concentration on the degradation efficiency of EBT dye at constant initial pH. The removal percentage increased proportionally with the increase of photocatalyst dosage due to enhancement in the generation of hydroxyl radicals. Higher catalyst loadings were antagonistic to the degradation, perhaps due to particle agglomeration, reduction in the available surface area for light absorption, and EBT adsorption [38,40]. On the other hand, the interaction effect of C-doped ZnO loading and the initial pH of the reaction mixture on the degradation of EBT dye is depicted in Fig. 9 (b). From the response surface, it can be seen that the degradation efficiency was low at acidic

pH value due to the loss of C-doped ZnO perhaps, whereas at alkaline medium the hydroxyl radicals played a positive role in the removal of EBT as earlier observed in the case of other organic contaminants [41]. The fact that the EBT dye has a pKa value of 6.6 and the pH_{pzc} of ZnO is 9 implies that interelectrostatic attraction is favored [42]. Lastly, the synergistic effect of EBT initial concentration and initial solution of pH in removing EBT dye is revealed by Fig. 9(c). However, the degradation efficiency is reduced with increasing EBT concentration due to the interception of the photon before they reach the surface of the C-ZnO photocatalyst. Moreover, the columbic repulsion between the negatively charged C-doped ZnO photocatalyst surface and hydroxyl anions at highly

alkaline conditions reduced the EBT removal rate via

suppression of the generation of hydroxyl radicals [43].

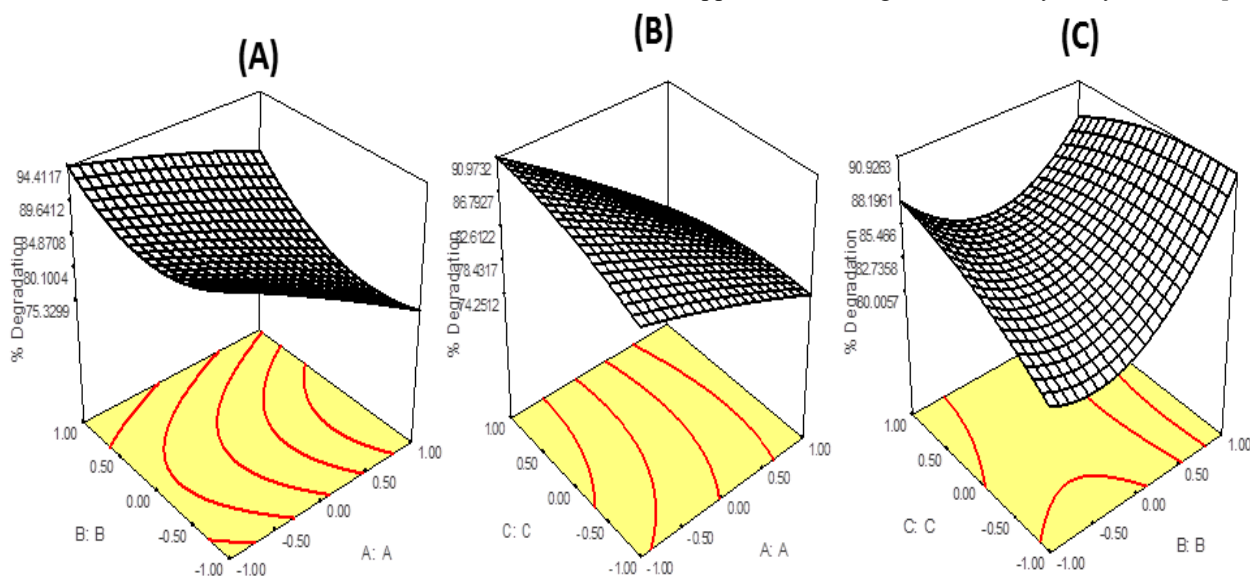


Fig. 9. The 3D response surfaces for the effect of: (A) initial concentration and catalyst dosage (B) initial concentration and initial pH (C) catalyst dosage and the initial pH.

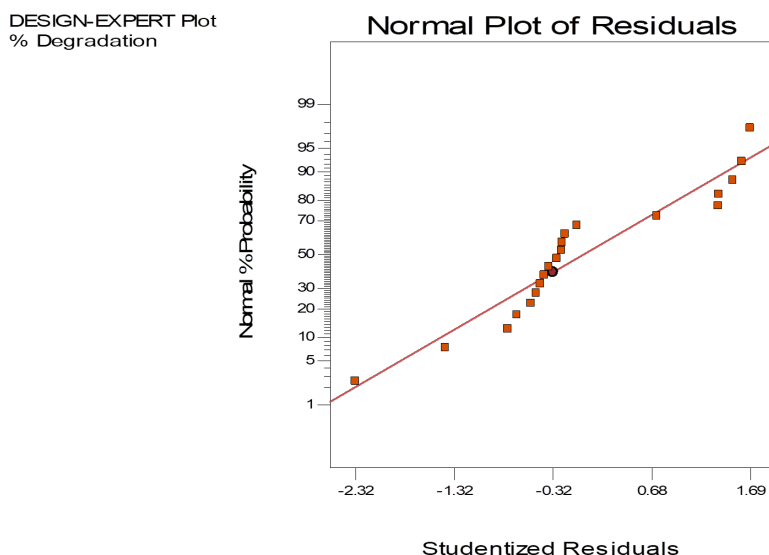


Fig. 10 A linear normal plot of residual for the modelled EBT degradation

The normal plot of residuals is displayed in Fig. (10). Based on the figure, the linearization of all the points along the line of the normal plot shows that the model, its effects and associated graphs are largely unaffected by noise.

3.5. Stability and Reusability of C-doped ZnO

To determine the reusability of the C-doped ZnO photocatalyst, experiments were performed based at the optimum conditions of the photocatalytic degradation of EBT over the C-doped ZnO. The residual catalyst from degradation experiment was filtered, washed and dried and then recycled in fresh experiment and the result was illustrated in Fig. 11.

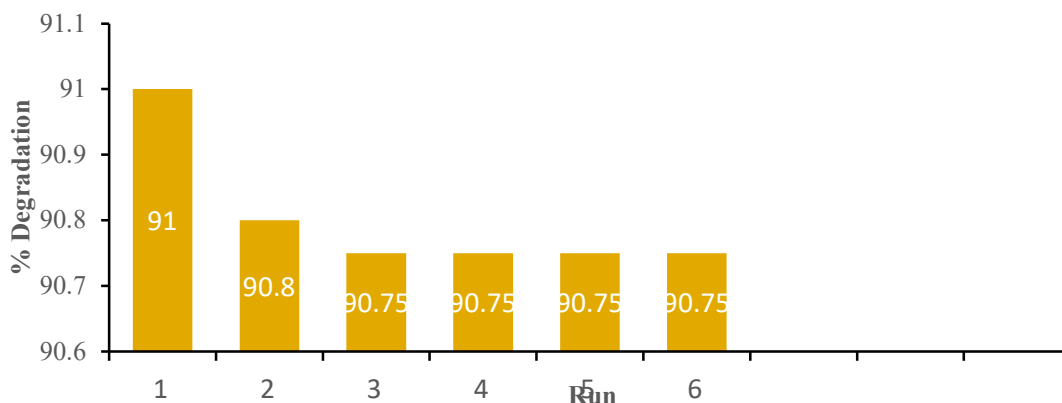


Fig. 11 Stability and reusability pattern of C-doped ZnO in the course of degradation of EBT

From figure 10 it can be seen that the degradation of eriochrome black T decreased steadily during the 1st and 2nd cycle but 3rd, 4th, 5th and 6th cycles remained the same. This clearly shows the stability and effectiveness of the C-doped ZnO photocatalyst in the degradation of eriochrome black T.

3.6. Comparative Study

Control experiments were conducted to evaluate the contribution of background reactions to the photocatalytic EBT removal over synthesized C-doped ZnO photocatalyst. The effects of irradiation time on the percentage removal of EBT over bare ZnO, C-doped ZnO, adsorption and photolysis over 100 min is shown in Fig. 12. From the figure, the adsorption of EBT in a suspension of 0.1 g/L catalyst at pH = 11 in the dark results in the removal of less than 19.45 % of this chemical compound due to the non-availability of hydroxyl radicals on the surface of the catalyst. In the photolysis, the percentage removal of EBT was 33 % probably due to the absence of

photocatalyst in the EBT solution. Conversely, the percentage removal of EBT by photocatalysis over the bare ZnO and C-doped ZnO were 86 % and 98 %, respectively, which clearly demonstrates that the as-synthesized C-doped ZnO photocatalyst has a better photoefficiency for the removal of EBT than the undoped ZnO catalyst. The excellent performance of the C-doped ZnO can be attributed to the possible contribution of photolysis, the suppression rate of recombination and the low band gap of this photocatalyst [44]. This however negates the results of Alshammari *et al.* [45] under ultraviolet light irradiation, which revealed that ZnO is more active than C-doped ZnO. In addition, the large specific surface area of C-doped ZnO (51.58 m²g⁻¹) may be partly responsible for the observed higher visible light photoactivity of C-doped ZnO when compared with that of undoped ZnO (34.62 m²g⁻¹). Generally, the photoefficiency of heterogeneous photocatalysis increases with an increase in the specific surface area of the photocatalyst.

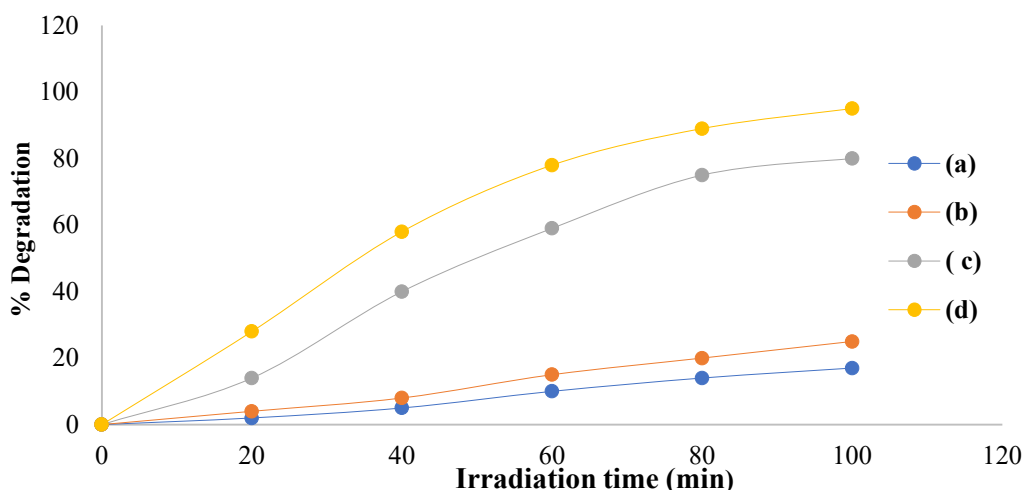


Fig. 12 Effect of irradiation time on the photocatalytic degradation of EBT under different processes. (a) Adsorption. (b) Photolysis. (c) Photocatalysis over undoped ZnO. (d) Photocatalysis with C-doped ZnO. Initial EBT 10 mg/L, catalyst dose = 0.1 g/L, and pH = 11

To evaluate the effect of irradiation time on the photocatalytic removal of EBT two control experiments were conducted under two different conditions of ultraviolet (UV) and visible light at optimal process parameters (5.00 mg/L EBT initial concentration, 0.1 g/L of catalysts (ZnO or C-ZnO), and initial pH of 11 and their results were displayed in Fig. 13 and Fig. 14 respectively. From the Fig.13, the percentage removal of EBT by photocatalysis over the undoped ZnO and C-doped ZnO

nanoparticles were 72 % and 80 %, respectively, which clearly demonstrates that the as-synthesized C-doped ZnO photocatalyst has a better photoefficiency for the removal of EBT than the undoped ZnO catalyst. The high photocatalytic activity of the C-doped ZnO can be attributed to more penetration as earlier obtained by Chang *et al.* [46] under similar conditions of ultraviolet light irradiation, which revealed that C-doped ZnO is more active than undoped ZnO nanoparticles.

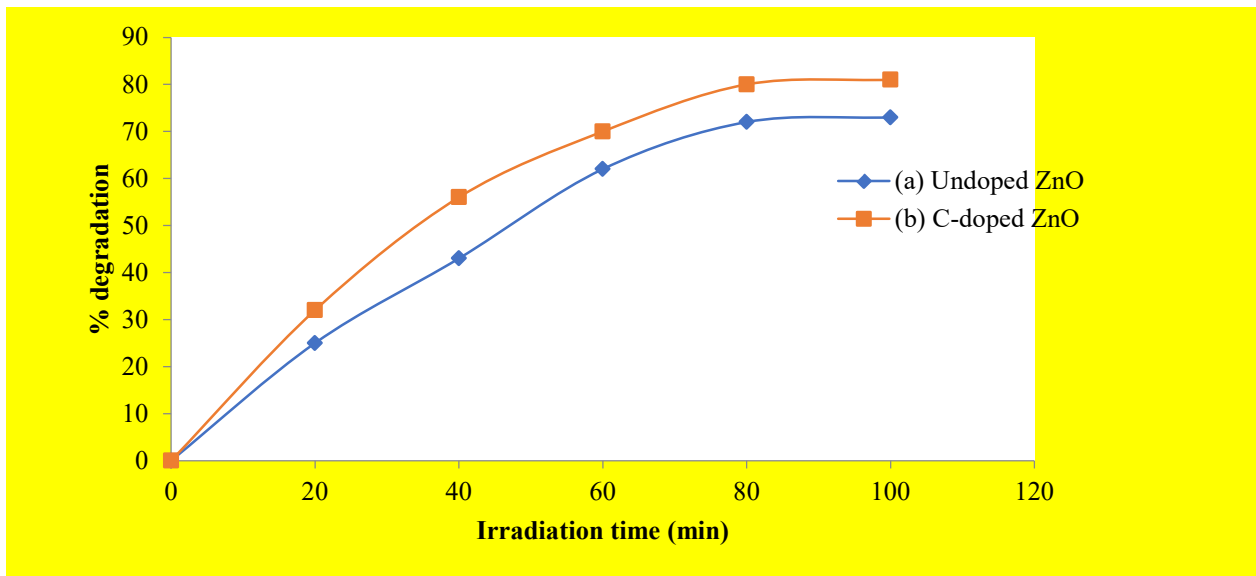


Fig. 13 Effect of irradiation time on the photocatalytic degradation of EBT under UV light irradiation (a) undoped ZnO (b) C-doped ZnO

Similarly, from Fig. 14 the percentage removal of EBT by photocatalysis over the undoped ZnO and C-doped ZnO nanoparticles were 61 % and 70 %, respectively, which clearly corroborates that the as-synthesized C-doped ZnO photocatalyst has a better photoefficiency for the removal of EBT than the undoped ZnO catalyst. The high photocatalytic activity of the C-doped ZnO can be attributed to the higher stimulation of nanoparticles by sunlight. This supports the results of Perillo and Atia [24]

under sunlight, which revealed that C-doped ZnO is more active than undoped ZnO nanoparticles (86% and 98 % in comparison to the results obtained under the UV irradiation), respectively. The findings of TAMILISA and PALANISAMY [47] also support the fact that the photocatalytic removal of EBT over C-doped ZnO nanoparticles under visible light irradiation shows higher photodegradation efficiency than the photodegradation under UV light.

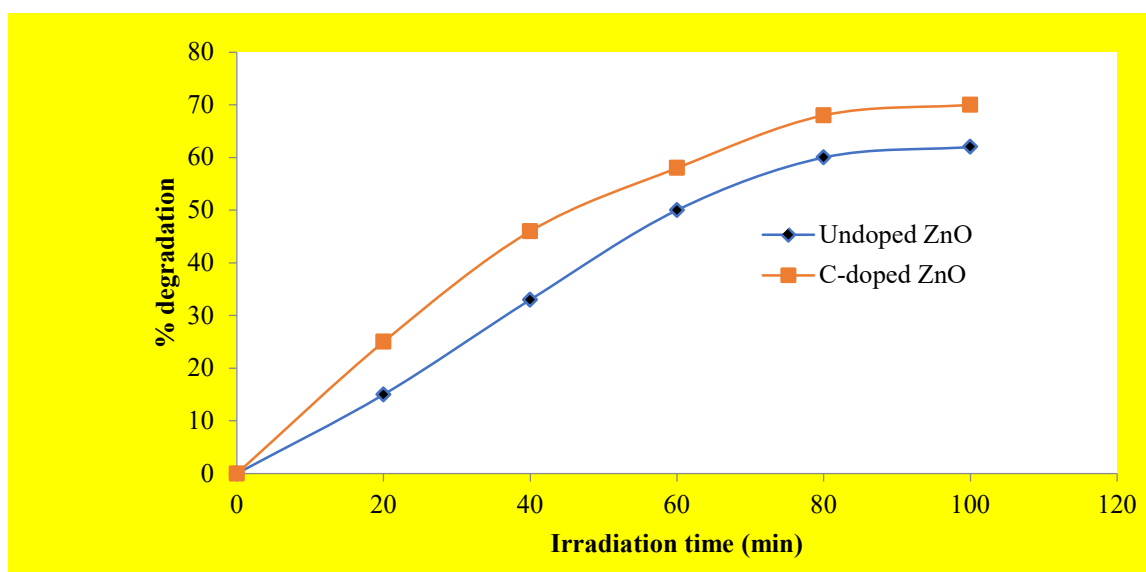


Fig. 14 Effect of irradiation time on the photocatalytic degradation of EBT under sunlight irradiation (a) undoped ZnO (b) C-doped ZnO

The analytical results obtained from XRD, SEM and UV/Vis spectrophotometry of the mechanochemically synthesized C-doped ZnO nanoparticles clearly show diminishing particles sizes while specific surface area increases relative to the undoped ZnO photocatalyst. Such increase in the surface area of the as synthesized C-doped ZnO nanoparticles can be linked to enhanced the interfacial photoreactions between the C-doped ZnO catalyst and the Eriochrome Black T. Similarly, the band gap energy for the C-doped ZnO has been reduced compared to that of the undoped ZnO nanoparticles. Accordingly, the lower the value of the band gap energy the greater the possibility to enhance the photocatalytic reactions [34]. Moreover, the UV-Vis spectral results of the as synthesized ZnO nanoparticles were consistent with the experiment results observed on the photocatalytic removal of Eriochrome Black T using photoresponsive C-doped ZnO nanoparticle.

3.6 Photodegradation rates and mechanism

The pseudo-first order integrated rate eq. (14) is widely used to model the kinetics of photocatalytic reactions [27].

$$\ln \frac{[C]_0}{[C]_t} = k_{app} t \quad (14)$$

Where C_0 and C_t are the initial and final concentration of EBT, k_{app} is the apparent rate constant and t is the illumination time (t) respectively. A plot of $\ln \frac{[C]_0}{[C]_t}$ versus t gave a straight-line graph with slope = k_{app} and R^2 values depicted in Fig. 15. The apparent rate constants are 0.0135, 0.0113, 0.0050 and 0.0015 min^{-1} , at various initial concentrations (5, 10, 15 and 20) and the R^2 values are adequate especially in the case of 20 mg/L EBT, indicating consistency of the photocatalytic degradation of eriochrome black T with the pseudo-first-order kinetics.

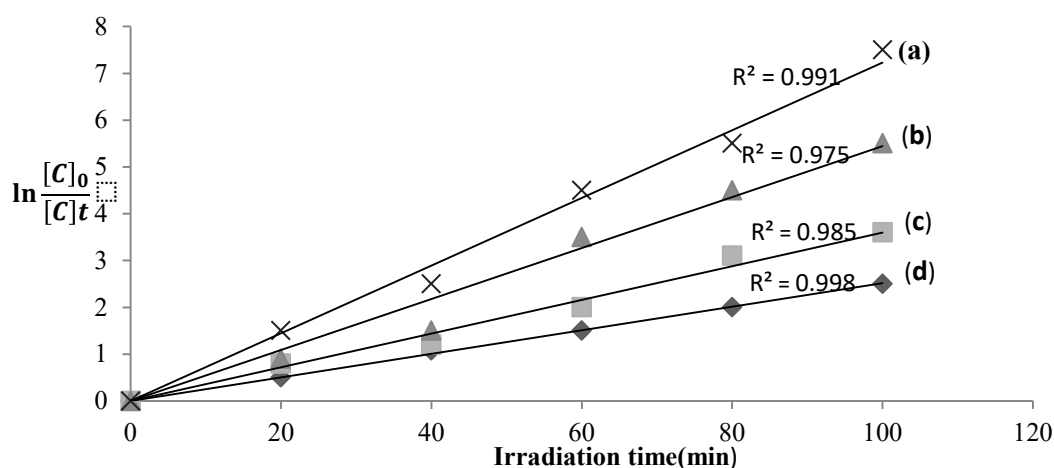


Fig. 15 Pseudo-first order kinetics plot for the photocatalytic degradation of EBT over C-doped ZnO at different concentrations. (a) 5 mg/L. (b) 10 mg/L. (c) 15 mg/L. (d) 20 mg/L

Generally, photocatalysis is based on the generation of electron-hole pairs upon light irradiation [20]. In this study, the electron migrates from the valence band to the conduction band, leaving behind a hole in the valence band which participates in redox reactions with the absorbed Eriochrome Black T dye and adsorbed molecular oxygen. On the other hand, the generation of electrons in the conduction band and holes in the valence band under visible light irradiation is not feasible owing to the wide band gap of ZnO (herein 3.25 eV).

As shown in Fig. 16, the incorporation of carbon into the ZnO lattice lead to the formation of a new, shorter mid-gap energy state, the C 2p band, above the O 2p valence band, which eventually shifted the optical absorption to the visible light region. As the figure shows, these lattice events make it possible for the electrons to migrate to the surface and the valence band of the C-doped ZnO, making it possible for photocatalytic reactions to occur [32]. These surface reactions include the formation of radical species such as $\text{O}_2^{\bullet-}$, HO^{\bullet} , HO_2^{\bullet} , H_2O_2 and singlet oxygen ($^1\text{O}_2$) [27], and their utilization in the conversion of EBT to mineral products.

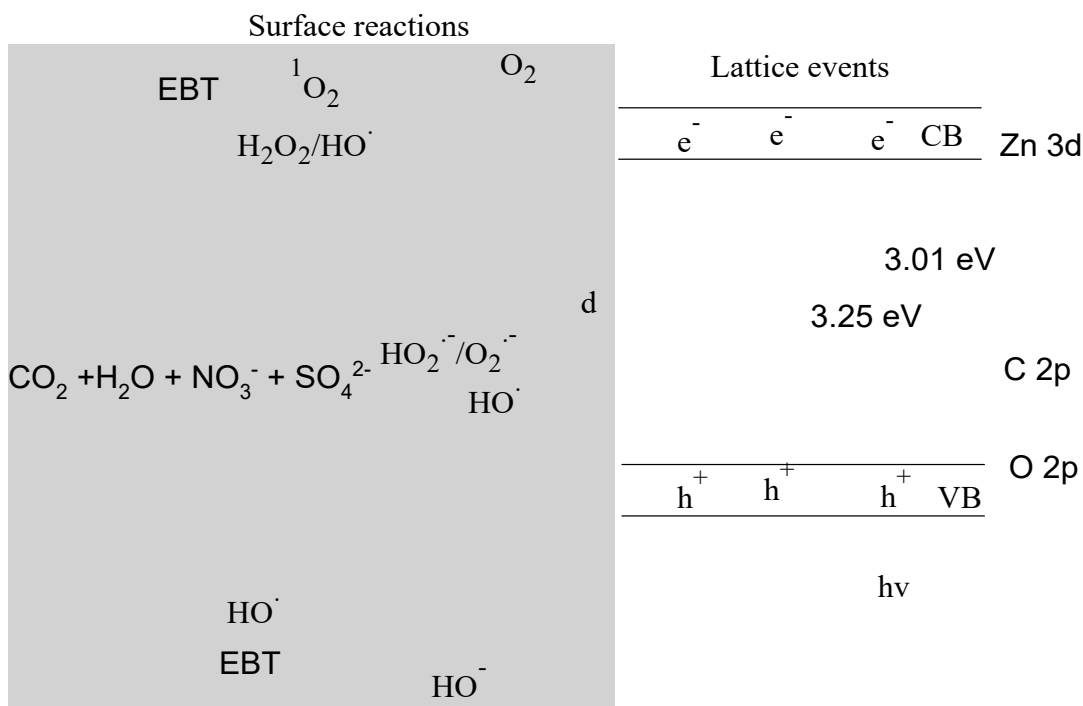
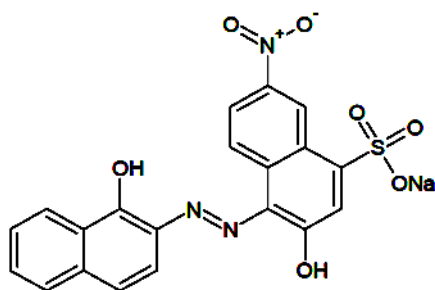


Fig. 16 The mechanism of EBT degradation in the presence of C-doped ZnO, under visible irradiation. The beauty of photodegradation reaction is the conversion of the pollutant (EBT) into environmental friendly species carbon (IV) oxide (CO_2), water (H_2O) and mineralized sulfate (SO_4^{2-}), carbonate (CO_3^{2-}), and nitrate (NO_3^-). Specifically, the final photodegradation products of EBT over C-doped ZnO photocatalyst are shown in eq. 15.



Acknowledgement: The authors thank the Department of Pure and Industrial Chemistry, Faculty of Physical Sciences Bayero University Kano, for providing most of the facilities required for this research work.

Competing interests

The authors declare that they have no competing interests.

References

[1] V. Vaiano, M. Matarangolo, O. Sacco, D. Sannino, Photocatalytic Removal of Eriochrome Black T Dye over ZnO Nanoparticle Doped with Pr, Ce or Eu, *Journal of Chemical Engineering. Trans.*, 2017, 57, 625-630.

[2] S. Kansal, S. Kumar, U. Swaiti, M.S.K. Ahmad, Photocatalytic Degradation of Eriochrome Black T Dye using well-Crystalline Anatase TiO_2 Nanoparticles, *Journal of Alloys Compounds*, 2013, 581, 392-397.

[3] J. Kaur, S. Singhal, Highly Robust Light Driven ZnO Catalyst for the Degradation of Eriochrome Black T at Room Temperature, *Super lattices Microstructure*, 2015, 83, 9-21.

[4] T.F. Saeid, F.F. Reza, A.R. Zolfa, Green Synthesis, Characterization and Photocatalytic Activity of Cobalt Chromite Spine Nanoparticles using Eriochrome Black T, *Mater. Res. Express*, 2019, 7(1), 2053-1591.

[5] U.G. Akpan, B.H. Hameed, Parameter Affecting the Photocatalytic Degradation of Dyes Using TiO_2 - Based Photocatalysts: A Review. *Journal of Hazardous Materials*, 2009, 170, 520-529.

- [6] S. Sharma, N. Chaturvedi, R.K. Chaturvedi, M.K. Sharma, Photocatalytic Degradation of Eriochrome Black T Using Ammonium Phosphomolybdate Semiconductor. *International Journal of Chemical Science*, 2010, 8(3), 1580-1590.
- [7] A.A. El-Bindary, A. Ismail, E.F. Eladi, Photocatalytic Degradation of Reactive Blue 21 Using Ag Doped ZnO Nanoparticle, *Journal of Material Environmental Science.*, 2019, 10(12), 1258-1271.
- [8] C. Tian, Q. Zhang, A. Wu, M. Jiang, M. Liang, B. Jiang, H. Fu, Cost-Effective Large-Scale Synthesis of ZnO Photocatalyst with Excellent Performance for Dye Photodegradation, *Chem. Commun*, 2012, 48, 2858-2865.
- [9] P. Franco, O. Sacco, I. Demarco, D. Sannino, V. Vaiano, Photocatalytic Degradation of Eriochrome Black T Azo Dye Using Eu-Doped ZnO Prepared by Supercritical Antisolvent Precipitation Route: A Preliminary Investigation, *Top. Catalysis*, 2020, 63(1), 1193-1205.
- [10] N.F. Djaja, R. Saleh, Characteristic and Photocatalytic Activities of Ce-Doped ZnO Nanoparticles. *Materials of Science Applied*, 2013, 04, 145-152.
- [11] S. Liu, J. Yu, Q. Xiang, Improved Visible-Light Photocatalytic Activity of Porous Carbon Self-Doped ZnO Nanosheet-Assembled Flowers, *Cryst. Eng. Comm*, 2011, 13(7), 2943-2949.
- [12] S. Benkhaya, S. M'rabet, A. El-Harfi, Classifications, Properties, Recent Synthesis and Application of Azo Dyes, *Heliyon*, 2020, 6(1) e03271.
- [13] R. Elshaarawy, T.M. Sayed, H.M. Khalifa, E.A.A. El-Sawi, Mild And Convenient Protocol For The Conversion of Toxic Acid Red 37 Into Pharmacological (Antibiotic and anticancer) Nominees: Organopalladium Architectures, *Compt. Rendus Chem*, 2017, 20, 934-941.
- [14] G. Jethave, U. Fegade, S. Attarde, S. Ingle, Decontamination Study of Eriochrome Black T from Wastewater by Using Altipbo Nanoparticles for Sustainable Clean Environment. *Journal of water Environmental Nanotechnology*, 2019, 4(4): 263-274.
- [15] I.N. Ismael, H.S. Wahab, Adsorption of Eriochrome Black T Azo Dye onto Nanosized Anatase TiO₂, *Am. J. Environ. Eng. Sci*, 2015, 2(6), 86-92.
- [16] M.D.G. De-luna, E.D. Flores, D.A.D. Genuino, C.M. Futralan, M.W. Wan, Adsorption of Eriochrome Black T Dye Using Activated Carbon Prepared from Waste Rice Hull-Optimisation, Isotherm and Kinetic Studies, *J. Taiwan Inst. Chem. Eng.*, 2013, 44, 646-653.
- [17] A. Sadollahkhani, I. Kazeminezhad, Photocatalytic Degradation of Eriochrome Black T Dye Using ZnO Nanoparticles. *Mater. Lett*, 2014, 120, 267-270.
- [18] K.M. Lee, S.B. Abdulhamid, C.M. Lai, Multivariate Analysis of Photocatalytic Mineralization of Eriochrome Black T Dye Using ZnO Catalyst and UV Irradiation, *Mater. Sci. Semi. Proc*, 2015, 39, 40-48.
- [19] D. Zhang, M.M. Wang, G. Han, S. Li, H. Zhao, B. Zhao, Z. Tong, Enhanced Photocatalytic Ability from C-Doped ZnO Photocatalyst Synthesized Without an External Carbon Precursor, *Fun. Mater. Lett*. 2014, 7(3), 1450026-1450030.
- [20] S. Yiwei, W. Hui, X. He, C. Lihui, H. Liulian, Preparation of Carbon Doped Zinc Oxide Induced by Nanocellulose and Its Photocatalytic Degradation Properties of Tetracycline. *Chem. Ind. For. Prod*, 2019, 39(5), 115-120.
- [21] Y.Y.G. Lim, K. Hsu, Y-C. Chen, L-C. Chen, S-Y. Chen, K-H. Chen, Visible-Light Driven Photocatalytic Carbon Doped Porous ZnO Nanoarchitecture for Solar Water Splitting, *Nanoscale*, 2012, 4, 6515-6519.
- [22] P. Rao, R.A. Chittora, B. Surbhi, Preparation and Application of Carbon Doped ZnO as Photocatalyst, *Acta Chim. Pharm. Indica*, 2015, 5(4), 143-150.
- [23] A.B. Lavand, Y.S. Malghe, Synthesis, Characterization and Visible-Light Photocatalytic Activity of Nanosized Carbon Doped ZnO, *Inter. J. Photochem*, 2015, 2015(2015), 1-9.
- [24] P.M. Perilla, M.A. Atia, C-Doped ZnO Nanorods for Photocatalytic Degradation of P-Aminobenzoic acid under Sunlight, *Nano-Struct. Nano-Objects*, 2017, 10, 125-130.
- [25] M. Shanthi, V. Kuzhalosai, Photocatalytic Degradation of an Azo Dye Acid Red 27 in Aqueous Solution Using Nano ZnO, *Indica. J. Chem*, 2012, 51(3), 428-434.
- [26] S. Mohammadzadeh, M.E. Olya, A.M. Arabi, A. Shariati, N.M.R. Khosravi, Synthesis, Characterization and Application of ZnO-Ag as a Nanophotocatalyst for Organic Compounds Degradation, Mechanism and Economic Study, *J. Environ. Sci*, 2015, 35, 194-207.
- [27] U.I. Gaya, Heterogeneous Photocatalysis using Inorganic Semiconductor Solids, *Springer. Dordrecht*, 2014.
- [28] K. Yoshio, A. Onodera, H. Satoh, N. Sakagami, H. Yamashita, Crystal Structure of ZnO: Li At 293 K and 19 K by X-ray Diffraction, *Ferroelectr*, 2001, 264(1), 133-138.
- [29] M. Bellardita, V. Augugliaro, V. Loddo, B. Megna, G. Palmisano, L. Palmisano, M.A. Puma, Selective Oxidation of Phenol And Benzoic Acid In Water Via Home-Prepared TiO₂ Photocatalysts: Distribution Of Hydroxylation Products, *Applied Catalysis A General*, 2012, 79-89.
- [30] A. Di Paola, E. Garcia-López, S. Ikeda, G. Marci, B. Ohtani, L. Palmisano, Photocatalytic Degradation of Organic Compounds in Aqueous Systems by Transition Metal Doped Polycrystalline TiO₂, *Catal. Today*, 2002, 75, 87-93.
- [31] A.H. Yusuf, U.I. Gaya, Mechanochemical Synthesis and Characterization of N-Doped TiO₂ for Photocatalytic Degradation of Caffeine, *Nanochem. Res*, 2018, 3(1), 29-35.
- [32] A.S. Alshammari, L. Chi, X. Chen, A. Bagabas, D. Kramer, A. Alromaeh, Z. Jiang, Visible-Light Photocatalysis on C-doped ZnO Derived from Polymer-Assisted Pyrolysis. *RSC. Adv*, 2015, 5(35), 27690-27689.
- [33] M. Kurban, I. Muz, Size-Dependent Adsorption Performance of ZnO Nanoclusters for Drug Delivery Applications. *Structural Chemistry (Springer)*, 2022, 4: 2063-2
<https://doi.org/10.1007/s11224-022-02063-2>.
- [34] M. Maruthupandy, M. Anand, G. Maduraiveeran, S. Suresh, A. Hameedha R. J. Priya, Investigation on the

Electrical Conductivity of ZnO Nanoparticles Decorated Bacterial Nanowires. *Adv. Nat. Sci. Nanosci. Nanotechnol.* 2016, 7(2016), 045011

[35] M.O Fatehah, H.A. Aziz, S. Stoll, Stability of ZnO Nanoparticles in Solution. Influence of pH, Dissolution, Aggregation and Disaggregation Effect, *J. Cataly. Sci*, 2014, 3(1), 75-84.

[36] M. Farrokhi, S.C. Hosseini, J.K Yang, S.M. Shirzad, Application of ZnO-Fe₂O₃ Nanocomposite on the Removal of Azo Dye from Aqueous Solutions, Kinetics And Equilibrium Studies, *Water,Air. Sol. Pollut*, 2014, 225(9), 115-118.

[37] C. Lu, Y. Wu, F. Mai, W. Chung, C. Wu, W. Lin, C. Chen, Degradation Efficiencies and Mechanism of ZnO – Mediated Photocatalytic Degradation of EBT under Visible-light Irradiation, *Journal of Catalysis Chemical Engineering*, 2009, 310(1-2), 159-165.

[38] R.H. Myers, D.C. Montgomery, Response Surface Methodology. Process and Product Optimization using Designed Experiments, *John Wiley and Sons. Inc*, 2002; 2nd edition.

[39] S. Chen, W. Zhao, W. Liu, H. Zhang, X. Yu, Preparation, Characterization and Activity Evaluation of p-n Junction Photocatalyst p-CaFeO₄-ZnO, *J. Chem. Eng.*, 2009, 155(1-2), 466-473.

[40] M.N. Chong, B. Jin, C.W.K. Chow, W.C. Saint, Recent Development in Photocatalytic Water Treatment Technology, *Water Res*, 2009, 44, 2997-3027.

[41] C. Shafiu, C. Lei, G. Shen, C. Gengyu, The Preparation of N-doped TiO₂-xNx by Ball Milling, *Chem. Phy. Lett*, 2005, 413(4), 404-409.

[42] N. Daneshvar, D. Salari, R.R. Khataee, Photocatalytic Degradation of Azo Dye Acid Red 14 in Water on ZnO as an Alternative Catalyst to TiO₂, *J. Photochem. Photobio*, 2004, 162(1-2), 317-322.

[43] A.H. Abdullah, H.J.M. Moey, H.Y. Azah, Response Surface Methodology Analysis of the Photocatalytic Removal of EBT using Bismuth Vanadate Prepared via Polyol Route, *J. Environ. Sci*, 2012, 24(9), 1694-701.

[44] E. Casbeer, V.K. Sharma, X.Z. Li, Synthesis and Photocatalytic Activity of Ferrites under Visible Light. *A rev. Sep. Purif. Technol*, 2011, 87, 1-14.

[45] A. Hamza, J.T. Fatuase, S.M. Waziri, O.A. Ajayi, Solar Photocatalytic Degradation of Phenol using Nanosized ZnO and α -Fe₂O₃, *Journal of Chemical Engineering Material Science*, 2013, 4(7), 87-92.

[46] Q. Q. Chang, Y. W. Cui, H. H. Zhang, F. Chang, B. H. Zhu, S. Y. Yu. C-doped ZnO decorated with Au Nanoparticles Constructed from the Metal Organic Framework ZIF-8 for Photodegradation of organic dye. *RSC Adv*, 2019, 9, 12689-12695.

[47] R. Tamilisa, P.N. Palanisamy, Review on the Photocatalytic Degradation of Textile Dyes and Antibacterial Activities of Pure and Doped ZnO. *International Journal of Research and Innovation in Applied Science (IJRIAS)*, 2018; 3(8); 2454-6194.